Applied Catalysis B: Environmental 324 (2023) 122278

Contents lists available at ScienceDirect

Applied Catalysis B: Environmental

journal homepage: www.elsevier.com/locate/apcatb

Porous sulfonyl binuclear carbonate poly(ionic liquid)s for one-pot fixation of diluted CO_2 into dimethyl carbonate

Jing Ding [a,*], Peiru Wang [a], Yuting He [a], Linyan Cheng [a], Xue Li [a], Cheng Fang [b], Hongping Li [c], Hui Wan [a,*], Guofeng Guan [a,*]

[a] State Key Laboratory of Materials-Oriented Chemical Engineering, College of Chemical Engineering, Jiangsu National Synergetic Innovation Center for Advanced Materials, Nanjing Tech University, Nanjing 210009, PR China
[b] College of Chemical Engineering, Nanjing Forestry University, Nanjing 210037, PR China
[c] Institute for Energy Research of Jiangsu University, Jiangsu University, Jiangsu 212013, PR China

ARTICLE INFO

Keywords:
Diluted CO_2
Sulfonyl binuclear carbonate
Poly(ionic liquid)s
Dimethyl carbonate
One-pot fixation

ABSTRACT

The direct utilization of diluted CO_2 skips the additional enrichment and purification operations required for high-purity CO_2, making it shine in the green catalytic process. However, achieving diluted CO_2 cycloaddition coupling transesterification with epoxide and methanol over poly(ionic liquids) catalyst and understanding the relevant mechanism at the molecular level are still challenging. Here, a novel porous sulfonyl binuclear carbonate poly(ionic liquid)s (SC-PILs) were successfully prepared by the integration of acidic monomers pre-polymerization with basic anions post-etching, regulating the chemical property of free anions and increasing the specific surface area of copolymerized materials. Relying on the synergy of the built abundant pores and the exposed basic anions, SC-PILs could one-pot efficiently catalyze the cycloaddition coupling transesterification reaction of the simulated flue gas (15% CO_2 + 85% N_2) without any co-catalyst, and dimethyl carbonate (DMC) with the yield of 80% was obtained. Theoretical studies deeply understood the activation difference of binuclear CO_3^{2-} anion on CO_2 compared with mononuclear CH_3COO^- anion and the ring-opening mechanism of [CO_3^{2-}+CO_2] adduct on epoxides, providing a better choice for high-value utilization of diluted CO_2 from flue gas.

1. Introduction

The dramatic increase of global CO_2 concentration has triggered a series of consequences, such as extreme climate, natural disasters, species withering and so on, posing a severe challenge to human survival and development [1–3]. However, the non-toxic, abundant and safe characteristics of CO_2 make it an ideal choice for organic synthesis module, injecting chemical power into the implementation of carbon neutralization strategy [4,5]. Among numerous catalytic pathways of CO_2, one-pot synthesis process coupling with CO_2 cycloaddition and CH_3OH transesterification has attracted extensive attention due to its wide application of green dimethyl carbonate (DMC) product in battery electrolyte, fuel additives, organic synthesis intermediates and other fields [6–9]. One-pot synthesis process can not only break the dilemma of thermodynamic stability of CO_2 with the addition of high-energy epoxides, but also omit the separation of intermediate products with the help of the bifunctionality of catalysts, so as to realize the win-win situation of carbon footprint recycling and catalytic process optimization [10,11].

Based on our previous works, the embedment of basic sites in catalysts has exhibited remarkable effects on the efficient activation of CO_2 and the smooth synthesis of DMC [12,13]. However, the high-purity CO_2 used mostly comes from the separation and purification of industrial flue gas (15% CO_2). This process always requires extra energy consumption and re-release CO_2, contradicting the concept of energy conservation and emission reduction [14,15]. Although the cycloaddition application of CO_2 from flue gas has been reported previously, the extensive use of co-catalysts (KBr, $ZnBr_2$, TBAB, etc.) increased the manufacturing cost and separation difficulty [16–19]. Considering the role of brominated additives in assisting the ring-opening of epoxides to facilitate the insertion of diluted CO_2, it coincides with the effect of basic sites to accelerate CO_2 activation. Therefore, adhering to the concept of green chemistry, it is of great significance for developing basic bifunctional catalysts without any co-catalyst to realize the directional conversion of

* Corresponding authors.
E-mail addresses: jding@njtech.edu.cn (J. Ding), wanhui@njtech.edu.cn (H. Wan), njutggf@163.edu.cn (G. Guan).

https://doi.org/10.1016/j.apcatb.2022.122278
Received 14 September 2022; Received in revised form 3 December 2022; Accepted 7 December 2022
Available online 9 December 2022
0926-3373/© 2022 Elsevier B.V. All rights reserved.

diluted CO_2 into DMC.

Poly(ionic liquid)s (PILs) integrate the functional characteristics of ionic liquid with polymer, providing a broad platform for adjusting the physicochemical properties of materials and designing effective catalytic processes [20,21]. Especially, the inherent nucleophilic halogen anions and polar imidazolium cations in PILs give them ideal catalytic ability for CO_2 cycloaddition reaction [22]. However, the absence of basic sites not only makes the traditional PILs unable to meet the effective activation of diluted CO_2, but also slows down the subsequent CH_3OH transesterification rate. Recently, basic carboxyl compounds are widely used in the field of CO_2 adsorption and activation, such as binary ILs mixture, acid-base amphoteric DESs, carboxyl ionic polymers, etc [23–25]. Nevertheless, PILs rich in acid-base and polar groups are easily to be pulled by hydrogen bonds, showing high viscosity in homogeneous system and non-porosity in heterogeneous system, resulting in limited exposure of functional sites. Consequently, it is necessary to explore the realization of pore making in the construction of basic bifunctional PILs.

In this context, sulfonyl binuclear carbonate functionalized poly (ionic liquid)s were rationally constructed by the combination of the acidic monomers pre-polymerization with basic anions post-etching, achieving the purpose of regulating the valence of basic anions and enhancing the specific surface area of copolymerized materials. The physicochemical properties of prepared materials were systematically investigated by various characterization, and the catalytic performance of SC-PILs in one-pot synthesis of DMC from simulated flue gas (15% CO_2 + 85% N_2) were detailedly studied without any co-catalyst. Moreover, with the help of DFT theoretical calculation, the bonding ability of binuclear carbonate anions to CO_2 and the ring-opening advantage of their adducts to epoxides were deeply explored.

2. Experimental section

2.1. Preparation of acidic ILs monomers

Typically, 1-(3-sulfopropyl)-3-vinylimidazole bisulfate ([PsVIm]HSO_4) was fabricated based on literature reported previously [26,27]. 20.0 mmol of 1-vinylimidazole and equimolar 1,3-propanesultone were respectively added into 10 mL of ethanol at 0 °C, and the above mixture was kept stirring for 24 h. Subsequently, the crude product was evaporated to remove ethanol, washed with ethyl acetate, and dried under vacuum overnight to produce [PsVIm]. ^{1}H NMR data was as follow: ^{1}H NMR (400 MHz, D_2O) δ (ppm) = 9.07 (s, 1 H), 7.77 (s, 1 H), 7.61 (s, 1 H), 7.13 (dd, *J*=15.6, 8.7 Hz, 1 H), 5.79 (dd, *J*=15.6, 2.8 Hz, 1 H), 5.41 (dd, *J*=8.7, 2.8 Hz, 1 H), 4.40 (t, *J*=7.1 Hz, 2 H), 2.93 (t, *J*=8.1, 2 H), and 2.37–2.30 (m, 2 H). Next, the acidification treatment was ongoing, 10 mmol of [PsVIm] was dissolved in 5 mL deionized water, and meanwhile the equimolar sulfuric acid was added dropwise to the above solution at 0 °C and then kept stirring at 60 °C for 24 h, followed by being evaporated to remove solvent and washed with ether to get wine-red [PsVIm]HSO_4.

1,4-butanediyl-3,3 '-divinylimidazole dihydrobromate ([C_4DVIm][HSO_4]$_2$) was prepared as follows: 20.0 mmol of 1-vinylimidazole and 10.0 mmol of 1,4-dibromobutane were put into 10 mL of methanol, and then the solution was refluxed for 24 h [28,29]. After cooling down, the crude product was evaporated, washed with ethyl acetate, and dried under vacuum to obtain [C_4DVIm]Br_2. The corresponding ^{1}H NMR was listed as follow: ^{1}H NMR (400 MHz, D_2O) δ (ppm) = 9.07 (s, 1 H), 7.78 (s, 1 H), 7.58 (s, 1 H), 7.13 (dd, *J*=15.6, 8.7 Hz, 1 H), 5.80 (dd, *J*=15.6, 2.8 Hz, 1 H), 5.42 (dd, *J*=8.7, 2.8 Hz, 1 H), 4.37–4.24 (m, 2 H), and 2.03–1.90 (m, 2 H). Then the anions exchange was ongoing, two equimolar sulfuric acid was added into 10 mmol of [C_4DVIm]Br_2 dropwise and was stirred in 10 mL of ice water. After feeding, the solution was kept stirring at 70 ℃ for 24 h under tiny reduced pressure to obtain reddish-brown [C_4DVIm][HSO_4]$_2$.

2.2. Preparation of functional SC-PILs materials

5 mmol of [PsVIm]HSO_4, 5 mmol of [C_4DVIm][HSO_4]$_2$, 10 mmol of divinylbenzene (DVB) and 1 mmol of 2, 2′-Azobis-(2-methylpropionitrile) were dissolved in the mixture of water and ethanol (15/45, mL/mL) and kept stirring at room temperature for 2 h (Scheme 1) [30,31]. Subsequently, it was treated at 100 °C for 24 h. Finally, the resulted white precipitate was obtained (named P-DPsC_4ImHSO_4) after filtering and washing with ethanol. Following a similar procedure, P-DPsIm ([PsVIm]/DVB=10 mmol/10 mmol), P-DC_4ImBr ([C_4DVIm]Br_2/DVB=10 mmol/10 mmol) and P-DPsC_4ImBr ([PsVIm]/[C_4DVIm]Br_2/DVB=10 mmol/10 mmol/10 mmol) were prepared.

In the process of carbonate anions exchange, 1.0 g of P-DPsC_4ImHSO_4 was stirred in 100 mL of 1.0 mol/L Na_2CO_3 solution at room temperature for 24 h. Subsequently, the white solid powder was obtained and washed with a certain of hot water till the filtrate was neutral. This operation was repeated three times to get P-DPsC_4ImCO_3. Following a similar preparation process, P-DPsC_4ImAc were synthesized by ion exchange of P-DPsC_4ImHSO_4 and CH_3COO^-.

2.3. Characterization and experimental measurements

The characterization, the synthesis of glycerol 1,2-carbonate (GLC) from glycidol (GO) and CO_2, one-pot synthesis of DMC from CO_2, glycidol (GO) and CH_3OH, the quantitative analysis of GLC and DMC (Fig. S1), ^{1}H and ^{13}C NMR characterization results of products after the cycloaddition reaction and after diluted CO_2 one-pot coupling reaction process (Fig. S1c–f) and DFT calculations were depicted in the ESI.

3. Results and discussion

3.1. Characterization of SC-PILs

P-DPsC_4ImCO_3 was prepared by acid monomers pre-polymerization followed with basic anions post-etching strategy (Scheme S1), and its physicochemical properties were systematically identified by different characterization.

Fourier transform infrared (FT-IR) spectra of SC-PILs was shown in Fig. 1a, exhibiting the group type and chemical composition within the polymeric framework. The stretching vibration peak of aliphatic C-H and the bending vibration peak of aromatic C-H appeared at around 2925 cm^{-1} and 710 cm^{-1}, implying all samples contained DVB units in their structures [32]. Comparing the spectral curves of P-DPsIm and P-DC$_4$ImBr, the characteristic peaks at 1040 cm^{-1} and 1250 cm^{-1} were respectively assigned to the stretching vibration of C-S and S═O in [PsVIm] unit, and the characteristic peak at 1160 cm^{-1} was assigned to the stretching vibration of C-N^+ in the structure of imidazolium cations [26,30,33]. After copolymerizing DVB, [PsVIm] and [C_4DVIm]Br_2 into P-DPsC_4ImBr, its characteristic peaks corresponded to those of functional monomers in Fig. S2. Furthermore, when both [PsVIm] and [C_4DVIm]Br_2 were treated with H_2SO_4 and then copolymerized with DVB to obtain P-DPsC_4ImHSO_4, the characteristic peaks of -OH in -SO_3H side-chain and S═O in HSO_4^- anions could be respectively detected at 615 cm^{-1} and 1115 cm^{-1}, indicating that acidic groups were successfully introduced [33]. After P-DPsC_4ImHSO_4 was exchanged by CH_3COO^- anions to obtain P-DPsC_4ImAc, the peaks at 615 cm^{-1} and 1115 cm^{-1} of acid group disappeared and were replaced by the symmetric and antisymmetric stretching vibration peaks of -COO^- groups at 1405 cm^{-1} and 1665 cm^{-1} [25]. However, after exchanging CO_3^{2-} anions with P-DPsC_4ImHSO_4 to obtain P-DPsC_4ImCO_3, the symmetrical stretching vibration signal of -COO^- groups red-shifted from 1405 cm^{-1} to 1345 cm^{-1}, attributed to the enhanced conjugation effect of the introduction of CO_3^{2-} anions. Moreover, the carbon-skeleton characteristics of typical P-DPsC_4ImHSO_4 and P-DPsC_4ImCO_3 were further confirmed by the solid-state ^{13}C NMR spectrum (Fig. 1b). Remarkably, the characteristic peaks at 29, 42, 128, 138 and 145 ppm were

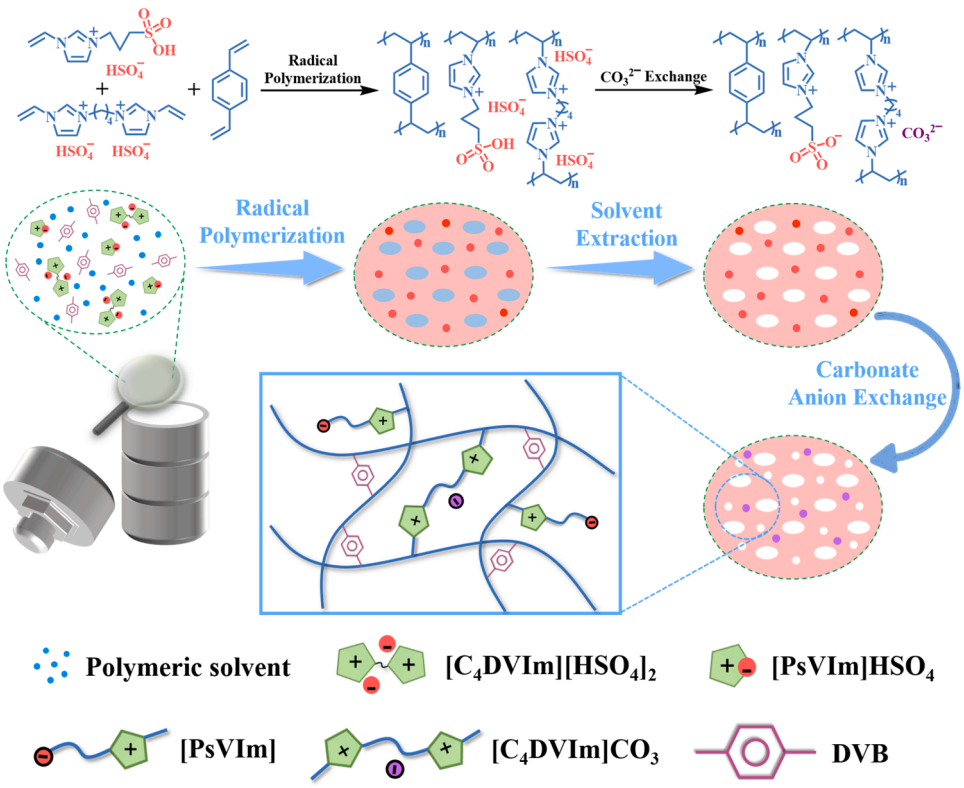

Scheme 1. Preparation process of SC-PILs.

respectively associated with the C signals of copolymerization main-chain (C13, C1), [PsVIm] unit side-chain methylene (C5, C6, C7), imidazolium ring (C2, C3, C4) and aromatic ring (C14, C15, C16) [26,34]. After P-DPsC_4ImHSO_4 was exchanged by CO_3^{2-} anions, the characteristic signal belonging to C12 appeared at 178 ppm, further indicating that CO_3^{2-} anions were successfully introduced. In addition, the appearance of characteristic peak for N heterocyclic carbene C centered at 164 ppm was ascribed to the stripping of acidic hydrogen proton at C2 position of imidazolium ring by the introduced CO_3^{2-} anions [35,36].

The chemical composition of SC-PILs and the O species chemical states towards P-DPsC_4ImCO_3 were studied by X-ray photoelectron spectroscopy (XPS) spectra. As shown in Fig. 1c, the signals at 531.4, 401.5, 284.5, 231.5 and 167.5 eV in full spectrum of P-DPsIm were respectively corresponded to the characteristic peaks of C 1 s, N 1 s, O 1 s, S 2 s and S 2p [26,37]. When $[C_4DVIm]Br_2$ and P-DPsIm copolymerized to obtain P-DPsC_4ImBr, the characteristic peaks of Br 3 s, Br 3p and Br 3d appeared at 257.0, 182.6 and 69.0 eV [38]. As shown in Fig. S3a, the N1s peaks at 402.0 eV and 399.8 eV were assigned to the C-N bonds of imidazole rings in PDPsC4ImBr, which was well consistent with literature reported previously [39]. Meanwhile, as observed in the Fig. S3b, the existence of the Br 3d signals in the XPS spectra of PDPsC4ImBr (67.1 eV) implied the successful copolymerization of monomers [PsVIm], $[C_4DVIm]Br_2$ and DVB to produce P-DPsC_4ImBr. After the copolymerized monomers were pre-treated with H_2SO_4, the signals of Br^- anions in P-DPsC_4ImHSO_4 disappeared, indicating that there was no Br^- anion in $[C_4DVIm][HSO_4]_2$ unit, eliminating the effects of residual halogen anions on the catalytic performance in the CO_2 coupling reaction. By further exchanging P-DPsC_4ImHSO_4 with CH_3COO^- anions and CO_3^{2-} anions respectively, the characteristic peak strengths of S 2 s and S 2p decreased significantly, while those of O 1 s, N 1 s and C 1 s remained stable. Moreover, as depicted in Fig. 1d, the O 1 s spectrum of P-DPsIm was divided into two peaks centered at 529.2 eV and 527.9 eV, which were respectively classified to S═O and S−O bonds of side-chain sulfonyl groups [40,41]. However, after CO_3^{2-} anions were introduced, two new signals of C═O and C−O bonds appeared at 531.4 eV and 527.5 eV, indicating the construction of stronger electronegative O^- sites. Thermal gravimetric (TG) analysis of P-DPsIm, P-DPsC_4ImHSO_4 and P-DPsC_4ImCO_3 revealed their initial pyrolysis temperature was about 280 °C (Fig. S4), significantly higher than that of one-pot coupling reaction.

N_2 adsorption-desorption isotherms was used to evaluate the specific surface area and porosity of SC-PILs (Fig. 1e and f). When introducing $[C_4DVIm]Br_2$ unit into P-DPsIm, the specific surface area of P-DPsC_4ImBr increased from 37 $m^2 \cdot g^{-1}$ to 104 $m^2 \cdot g^{-1}$, indicating that the morphology could be effectively controlled by adjusting the polarity of copolymeric framework (Table S1), so as to improve the specific surface area. When the acid-base sites were constructed, the specific surface area of P-DPsC_4ImHSO_4 (98 $m^2 \cdot g^{-1}$) decreased slightly due to the traction of intermolecular hydrogen bonds. When P-DPsC_4ImHSO_4 was exchanged with different basic anions, the specific surface areas of P-DPsC_4ImAc (119 $m^2 \cdot g^{-1}$) and P-DPsC_4ImCO_3 (193 $m^2 \cdot g^{-1}$) increased. The reasons for the significant increase in specific surface area of P-DPsC_4ImCO_3 were as follows: (1) the stripping of H_2SO_4 molecule tethered at side-chain of [PsVIm]HSO_4 unit; (2) the substituting of double HSO_4^- anions by single CO_3^{2-} anion in $[C_4DVIm][HSO_4]_2$ unit [42,43]. The application of basic anions etching strategy could effectively construct abundant pores in the framework of P-DPsC_4ImCO_3, resulting in the increase of pore volume (0.16 $m^3 \cdot g^{-1}$) and the decrease of average pore size (3.4 nm). Meanwhile, P-DPsC_4ImCO_3 provided higher CO_2 adsorption capacity than other PILs (Fig. 1f). The order of corresponding CO_2 adsorption capacity was as follows: P-DPsC_4ImCO_3 (14.81 $cm^3 \cdot g^{-1}$) > P-DPsC_4ImAc (13.00 $cm^3 \cdot g^{-1}$) > P-DPsC_4ImBr (12.18 $cm^3 \cdot g^{-1}$) > P-DPsC_4ImHSO_4 (9.37 $cm^3 \cdot g^{-1}$), which was consistent with the Knoevenagel condensation results and CO_2-TPD results used to evaluate the basicity of the catalysts (Fig. S5). Elemental analysis is a good method to reveal the total chemical composition of SC-PILs samples. From Table S2, it could be clearly seen that the sulfur content of P-DPsC_4ImHSO_4 was highest (up to 4.362%). Compared with P-DPsC_4ImBr, the increase of sulfur content in P-DPsC_4ImHSO_4 was mainly attributed to the ion exchange of bromine ions by hydrogen

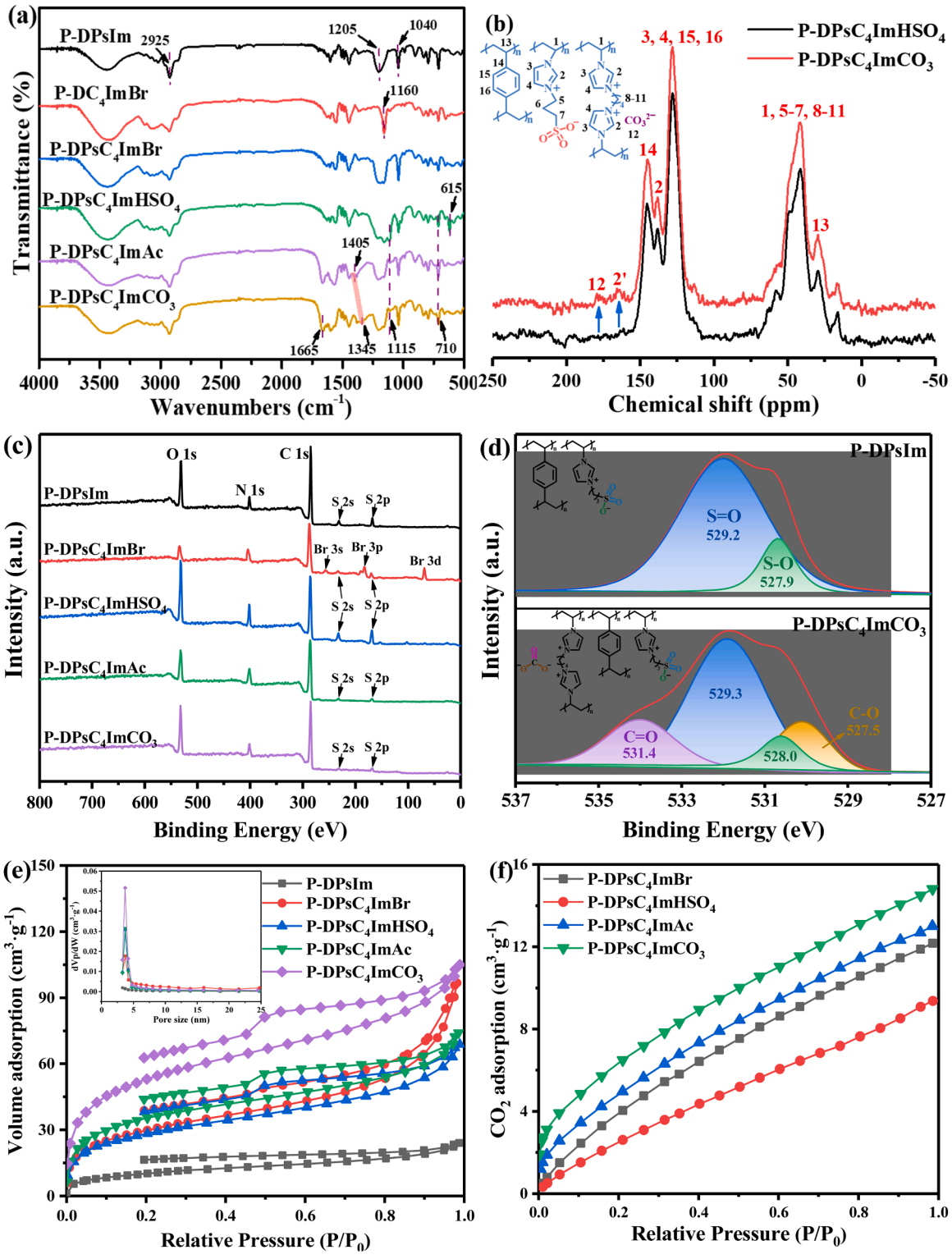

Fig. 1. (a) FT-IR spectra of as-prepared PILs. (b) Solid-state ^{13}C NMR spectra of P-DPsC$_4$ImHSO$_4$ and P-DPsC$_4$ImCO$_3$. (c) Full XPS spectra of as-prepared PILs. (d) High-resolution O1s XPS spectra of P-DPsIm and P-DPsC$_4$ImCO$_3$, (e) N_2 sorption-desorption isotherms of functional PILs. (f) CO_2 adsorption isotherms of functional PILs.

sulfate ions. Meanwhile, the sulfur content of P-DPsC$_4$ImCO$_3$ was lower than that of P-DPsC$_4$ImHSO$_4$, but the carbon content of P-DPsC$_4$ImCO$_3$ was higher than that of P-DPsC$_4$ImBr. This further verified that hydrogen sulfate was exchanged by carbonate. Moreover, the sulfur content of P-DPsC$_4$ImCO$_3$ was also lower than that of P-DPsC$_4$ImBr, which was attributed to that P-DPsC$_4$ImBr also contained some hydrogen sulfate, which was further exchanged by carbonate.

The morphology of SC-PILs was exhibited in Fig. 2. P-DPsIm prepared by solvothermal method of [PsVIm] with DVB, appeared as stacked spherical particles. When binuclear [C$_4$DVIm]Br$_2$ monomer was introduced into the framework of P-DPsIm to adjust the polarity of copolymeric components, the particle size of P-DPsC$_4$ImBr could be

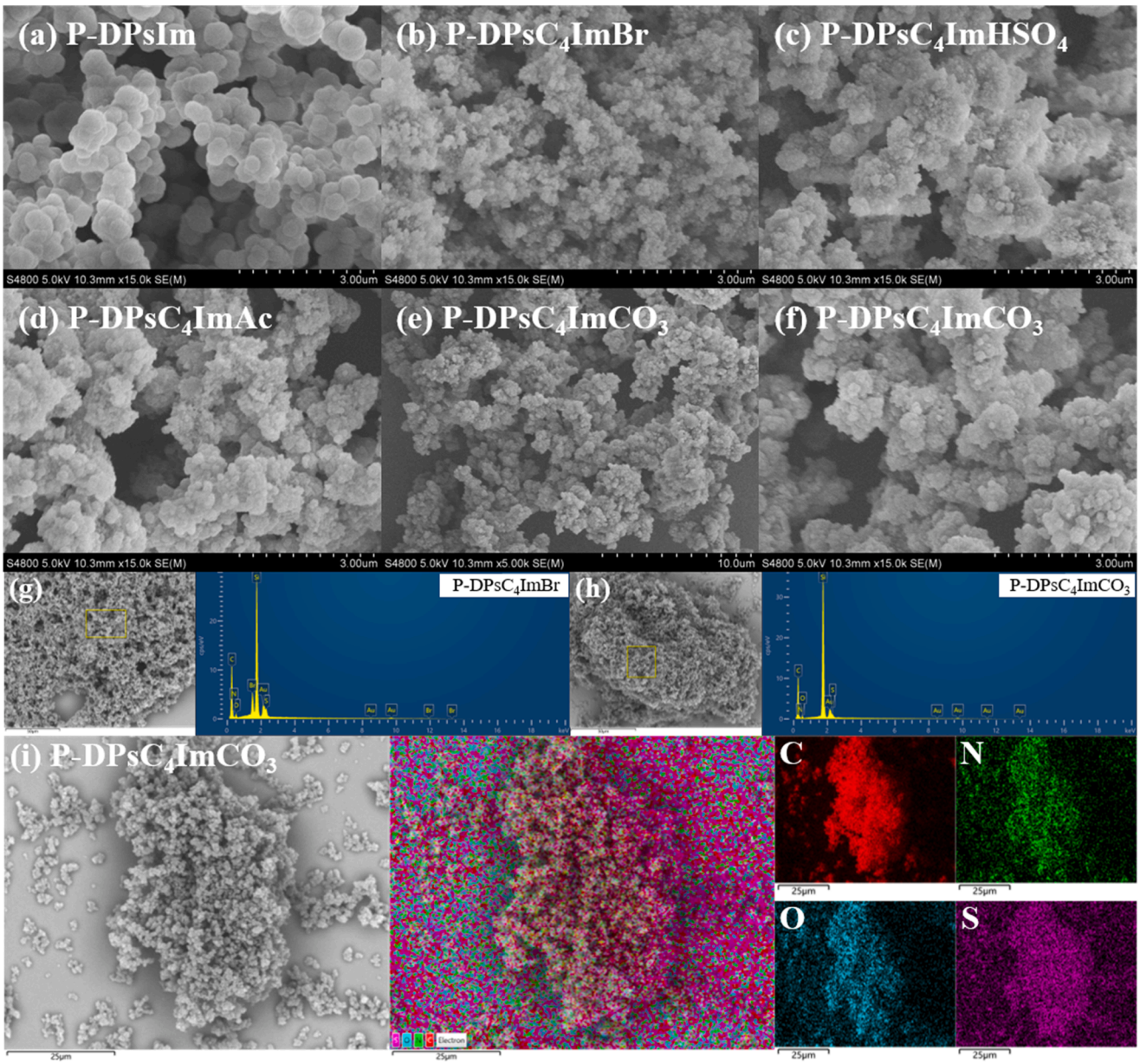

Fig. 2. Scanning electron microscopy (SEM) of (a) P-DPsIm, (b) P-DPsC4ImBr, (c) P-DPsC4ImHSO$_4$, (d) P-DPsC4ImAc, (e) and (f) P-DPsC4ImCO$_3$; The energy dispersive spectrometry (EDS) of (g) P-DPsC4ImBr and (h) P-DPsC4ImCO$_3$; and (i) the element mapping images of P-DPsC4ImCO$_3$.

effectively reduced. Obtaining from the copolymerization of [PsVIm]HSO_4, [C_4DVIm][HSO_4]$_2$ and DVB, the particles of P-DPsC_4ImHSO_4 were bonded into blocks due to the traction of intermolecular hydrogen bond. After HSO_4^- anions in P-DPsC_4ImHSO_4 were respectively replaced with CH_3COO^- anions and CO_3^{2-} anions, the morphology of P-DPsC_4ImAc and P-DPsC_4ImCO_3 changed unobviously, further illustrating the stability of polymeric framework. For the energy dispersive spectrometry (EDS) of P-DPsC_4ImCO_3, there was no obvious signal assigned to Br^- anions, further eliminating the effects of halogen anions on the catalytic activity. Moreover, element mapping images of P-DPsC_4ImCO_3 exhibited that C, N, O and S elements were uniformly dispersed, indicating the uniform distribution of polymeric units in the whole skeleton.

3.2. Performances of SC-PILs in one-pot coupling reaction

Without any co-catalyst and solvent, SC-PILs were used to one-pot cycloaddition coupling transesterification reaction of diluted CO_2 (15%) from simulated flue gas to study the diluted CO_2 chemical fixation of different functional groups of PILs. The detailed one-pot coupling reaction process was shown in Fig. S6. The first-step cycloaddition reaction of diluted CO_2 over different SC-PILs was performed. As exhibited in Table 1, selecting Glycidol (GO) as the epoxide substrate model, the yields of glycerol 1,2-carbonate (GLC) over P-DPsIm and P-DC4ImBr were respectively 11% and 60%, indicating the necessity of nucleophilic anions in CO_2 cycloaddition reaction. When [PsVIm] and [C_4DVIm]Br_2 were copolymerized into P-DPsC_4ImBr, the yield of GLC increased to 69%, which was attributed to the effective affinity of side-chain sulfonyl groups (-SO_3^-) to diluted CO_2. Moreover, P-DPsC_4ImAc and P-DPsC_4ImCO_3 obtained by basic anions exchange respectively exhibited the GLC yield of 83% and 92%, verifying the importance and necessity of basic sites. Furthermore, the first-step cycloaddition reaction condition of diluted CO_2 over P-DPsC4ImCO_3 was optimized and the optimal cycloaddition reaction conditions were obtained as follows: the reaction temperature 80 °C, the reaction pressure 20 bar 15% CO_2, the reaction time 2 h, the catalyst amount 50 mg. Under such condition, the yield of GLC over P-DPsC_4ImCO_3 was 97%.

Table 1
The catalytic activity of SC-PILs for diluted CO_2 one-pot coupling reaction.

Entry	PILs	First-step cycloaddition reaction		Subsequent Transesterification reaction	
		GLC Sel. (%)	GLC Yield (%)	DMC Yield (%)	By-product Yield (%)
1[a]	P-DPsIm	99	11	3	68
2[a]	P-DC_4ImBr	99	60	Trace	28
3[a]	P-$DPsC_4$ImBr	98	69	17	20
4[a]	P-$DPsC_4ImHSO_4$	99	32	16	50
5[a]	P-$DPsC_4$ImAc	98	83	55	14
6[a]	P-$DPsC_4ImCO_3$	98	92	68	6
7[b]	P-$DPsC_4ImCO_3$	98	97	80	Trace

[a] Initial cycloaddition conditions: 80 °C, 20 bar 15% CO_2, 2 h, 50 mg catalyst; Initial transesterification conditions: 140 °C, without CO_2, 1.0 h, 10 mol/mol CH_3OH/GO.
[b] Optimal cycloaddition conditions: 80 °C, 20 bar 15% CO_2, 3 h, 50 mg catalyst; Optimal transesterification conditions: 120 °C, without CO_2, 1.0 h, 15 mol/mol CH_3OH/GO.

After the CO_2 cycloaddition reaction under optimal reaction conditions, the unreacted CO_2 in the reaction system was released, and then methanol was added into the reaction system without the requirement of catalyst separation to further investigate the catalytic transesterification performance. For P-$DPsC_4$ImBr, it was found that only 17% DMC yield was obtained. The acidic copolymer P-$DPsC_4ImHSO_4$ only presented 16% DMC yield, indicating the importance of basic sites in the chemical fixation of diluted CO_2. The DMC yield of P-$DPsC_4ImCO_3$ (68%) was higher than that of P-DPsC4ImAc (55%), and only a small amount of GO left by cycloaddition reaction was alcoholized by CH_3OH (6%). Moreover, under the optimal subsequent transesterification reaction conditions (Figs. S7 and 3), the maximum yield (80%) of DMC over P-$DPsC_4ImCO_3$ was obtained. To illustrate the importance of sulfonyl group, the comparison of the catalytic performance of P-DC_4ImCO_3 and P-$DPsC_4ImCO_3$ was carried out. As shown in Fig. S8, the GO conversion and DMC yield of P-$DPsC_4ImCO_3$ (99% and 80%) was higher than that of P-DC_4ImCO_3 (81% and 62%) under the same reaction conditions. This could be attributed to the existence of the CO_2- sulfonate interaction that effectively enhanced the contact probability between CO_2 and active center in the structure of P-$DPsC_4ImCO_3$ and improved catalytic performance. Similar phenomena were reported in the previous literature [44,45].

Epichlorohydrin (ECH) and styrene oxide (SO) were chosen as the epoxide substrate for diluted CO_2 cycloaddition to study the comparison of catalytic activity with those in previous work, and its reaction conditions over P-$DPsC_4ImCO_3$ and the catalytic activity of partial reported PILs were shown in Table S3 [46–51]. It could be seen that both the yield of cyclic carbonate over P-$DPsC_4ImCO_3$ and its corresponding reaction condition were comparable or even better than that of PILs or other heterogeneous catalysts.

3.3. Linear carbonates universality and catalysts reusability

In view of the enhanced chemical stability of monohydric alcohol with the increase of length of alkyl chain, the reaction temperature and reaction time should be appropriately increased in the activity evaluation of diethyl carbonate and dipropyl carbonate. As shown in Fig. 4, under the optimal CO_2 cycloaddition reaction condition and the subsequent optimal transesterification reaction condition, more than 80% yield of the symmetrical carbonates was obtained. In addition, the activity evaluation of mixed alcohol system revealed that the yields of the asymmetric linear carbonates ranged from 39% to 45%.

The reusability of P-$DPsC_4ImCO_3$ was further investigated by carrying out recycling experiments of diluted CO_2 in one-pot coupling reaction. As shown in Fig. 5a, the DMC yield of P-$DPsC_4ImCO_3$ in one-pot

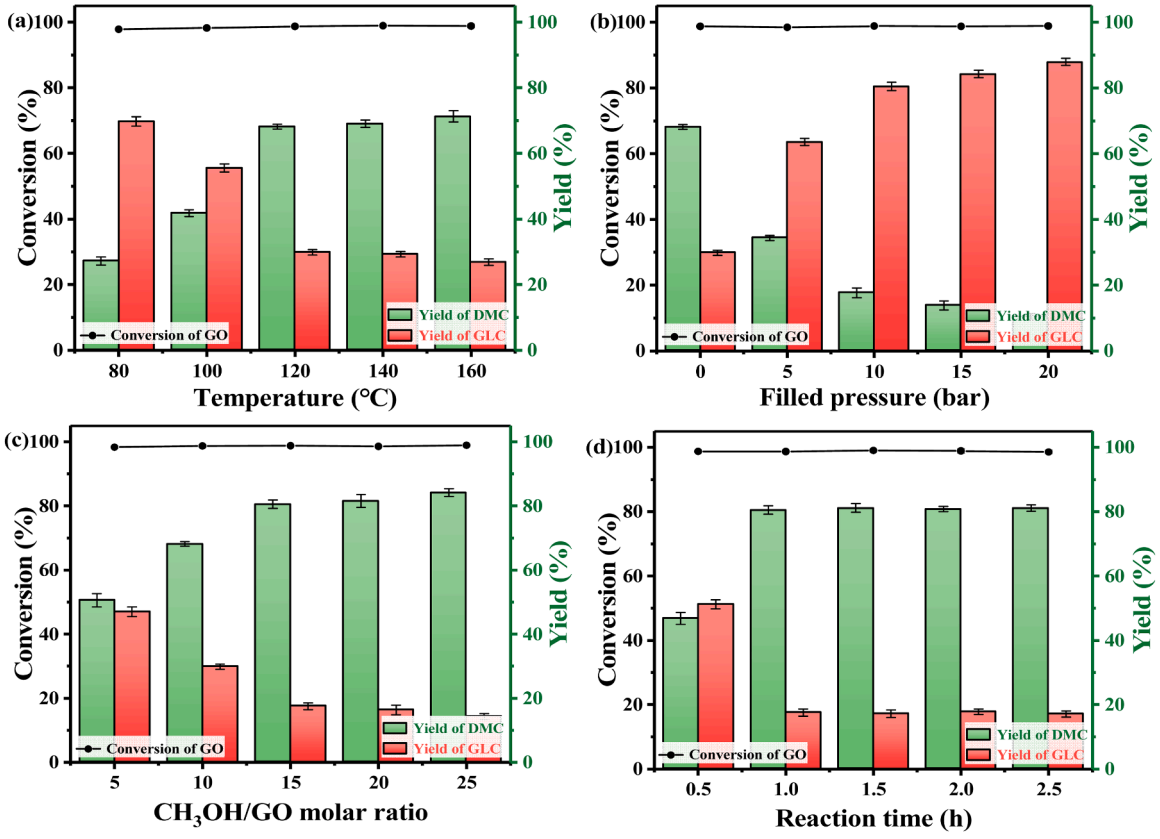

Fig. 3. Influences of different reaction process conditions on one-pot coupling reaction: (a) reaction temperature; (b) 15% CO_2 filled pressure; (c) CH_3OH/GO molar ratio; (d) reaction time.

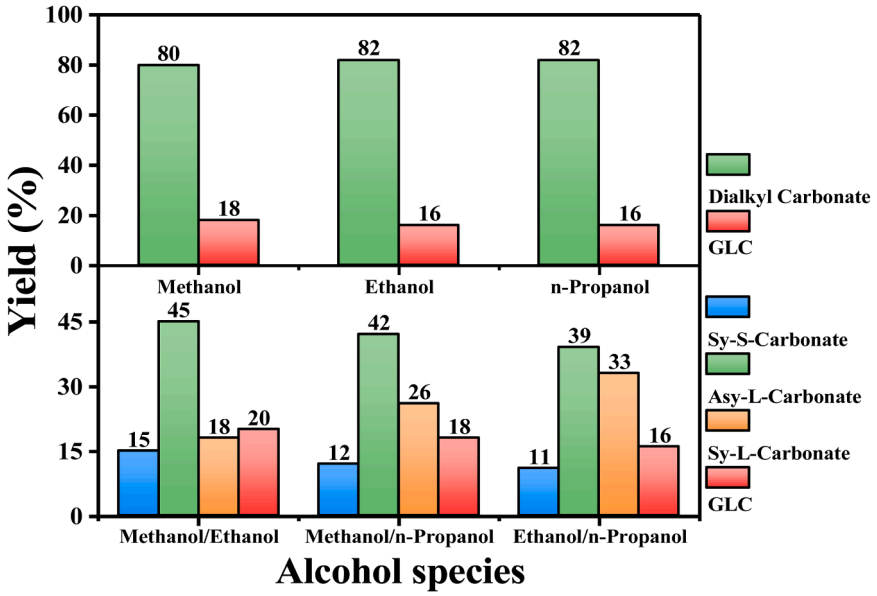

Fig. 4. Alcohol universality for synthesis of linear carbonates by one-pot coupling reaction (Sy-S-Carbonate is the abbreviation of symmetrical short-linear carbonate; Asy-L-Carbonate is the abbreviation of asymmetrical linear carbonate; Sy-L-Carbonate is the abbreviation of symmetrical long-linear carbonate.)

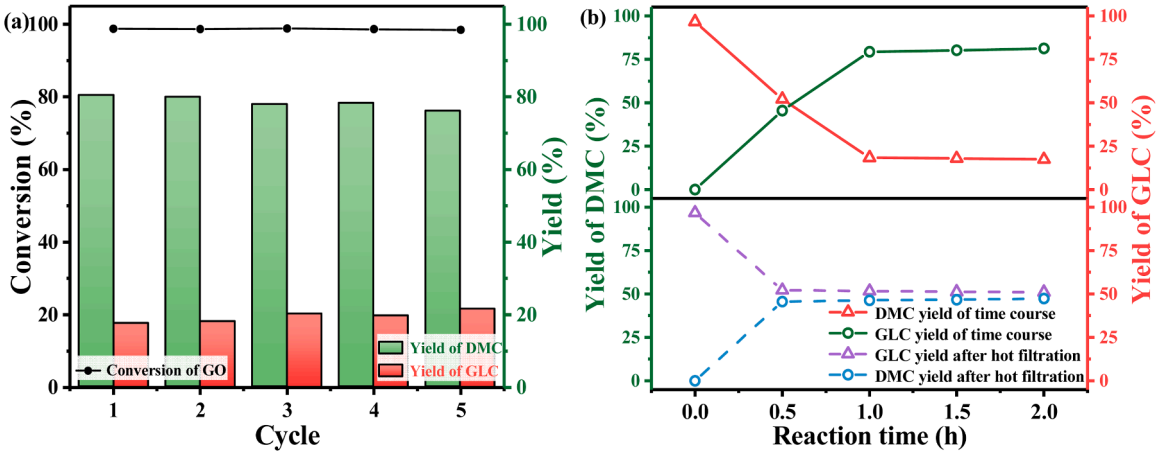

Fig. 5. (a) Stability evaluation of P-DPsC$_4$ImCO$_3$ and (b) Hot filtration tests of the transesterification subsequent reaction over P-DPsC$_4$ImCO$_3$ after diluted CO_2 cycloaddition reaction.

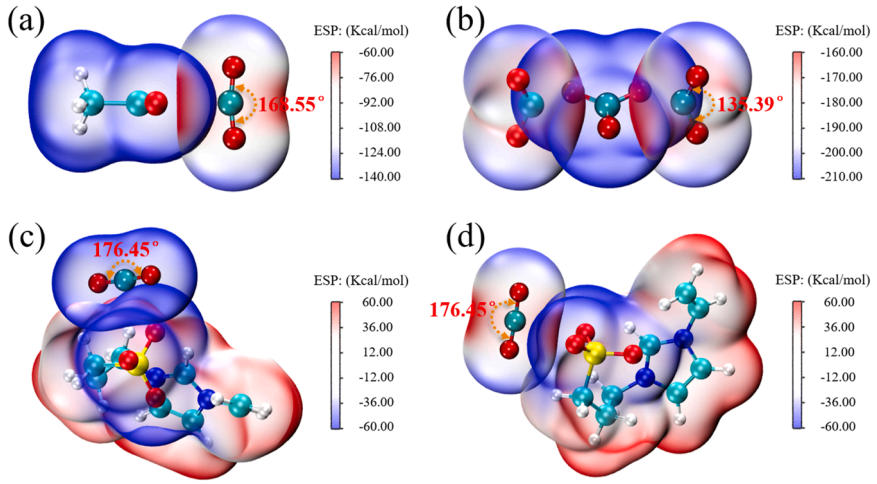

Fig. 6. ESP analysis of ionic sites with CO_2: (a) CH_3COO^-+CO_2, (b) CO_3^{2-}+2CO_2, (c)/(d) [PsVIm]+CO_2.

coupling reaction decreased by less than 5% after five runs, reflecting that P-DPsC$_4$ImCO$_3$ catalyst possessed good reusability. As for the slight deactivation during the recycling, it may be attributed to the blockage and collapse of the pore structure of the P-DPsC$_4$ImCO$_3$ catalyst during the catalysis reaction process (Fig. S9 and Table S4). To exclude the possibility of dissolution of active components, removing P-DPsC$_4$ImCO$_3$ by thermal filtration at CH$_3$OH transesterification process, the change of DMC yield was continuously monitored. As shown in Fig. 5b, after P-DPsC$_4$ImCO$_3$ was filtered out from the reaction system, there was no significant increase in DMC yield in the subsequent reaction period, illustrating that the active component stably existed in the polymerization framework. Compared with fresh P-DPsC$_4$ImCO$_3$, the reused P-DPsC$_4$ImCO$_3$ did not change obviously in FT-IR spectra (Fig. S10).

3.4. Study of the catalytic reaction mechanism

In order to explore the effective activation of ionic groups on CO_2, electrostatic potential analysis was applied to clarify the intermolecular electrostatic interaction. As shown in Fig. 6, CO_2 was affinity to the single carboxyl site of CH_3COO^- anion, and its molecular configuration was bent from linear equilibrium to 168.55 °. The symmetrical double carboxyl sites of CO_3^{2-} anion could both attract CO_2 and bend its linear bond angle to 135.39 °, which was significantly higher than that of the activation of CO_2 by CH_3COO^- anion. The -SO^{3-} site of the side chain of [PsVIm] unit could also activate CO_2, but the bond angle of CO_2 was only bent to 176.45 °, indicating that the weak basicity of -SO^{3-} site [52,53]. In view of the efficient activation of CO_2 by CO_3^{2-} anion, the interaction region indicator (IRI) diagram was drawn to better understand the types of non-covalent interaction between CO_3^{2-} anion with CO_2, in which the green region stood for weak van der Waals interaction, the blue one stood for strong electrostatic interaction and the red one stood for strong spatial repulsion [54–56]. As shown in Fig. 7a and b, CO_3^{2-} anion could be bonded with monomolecular or bimolecular CO_2 respectively, and produced corresponding peaks (< −0.15 a.u.) within the range of strong electrostatic interaction, indicating the formation of carbonate ionic adducts. In addition, there was also obvious hydrogen bonding between CO_3^{2-} anion with CH_3OH, which could stretch the bond length of O-H in CH_3OH from 0.9651 Å to 1.0045 Å, indicating the dissociation of CO_3^{2-} anion on CH_3OH molecule.

The electron delocalization ability of the above ionic groups and their CO_2 adducts was further evaluated by average local ionization energy (ALIE) analysis to assess the active sites in the coupling reaction [57,58]. As shown in Fig. S11, the ALIE minimal points of CH_3COO^- anion, CO_3^{2-} anion and [PsVIm] unit all existed at the carboxyl (-COO^-) or sulfonyl (-SO^{3-}) groups, which were respectively 4.16 eV, 2.34 eV and 10.18 eV, indicating that these were the weakest points for electron binding and were more prone to nucleophilic reaction. Combining with higher activation and bonding ability of CO_3^{2-} anion to CO_2 in ESP and IRI analysis, the ALIE minimal points of monomolecular CO_2 adduct [CO_3^{2-}+CO_2] and bimolecular CO_2 adduct [CO_3^{2-}+2CO_2] had also been analyzed. However, it was found that the ALIE minimal points were transferred to the bonded carbonate adducts region, which were respectively 1.59 eV and 3.31 eV, indicating that CO_3^{2-} anion could carry CO_2 to directly participate in the reaction.

For giving consideration to the simplicity of the models and the accuracy of the results, the corresponding imidazolium cation model was constructed according to the valence of nucleophilic anion, so as to reach a good balance between the accuracy of experiment and the low cost of calculation. As shown in Fig. 8a, the hydrogen proton at C2

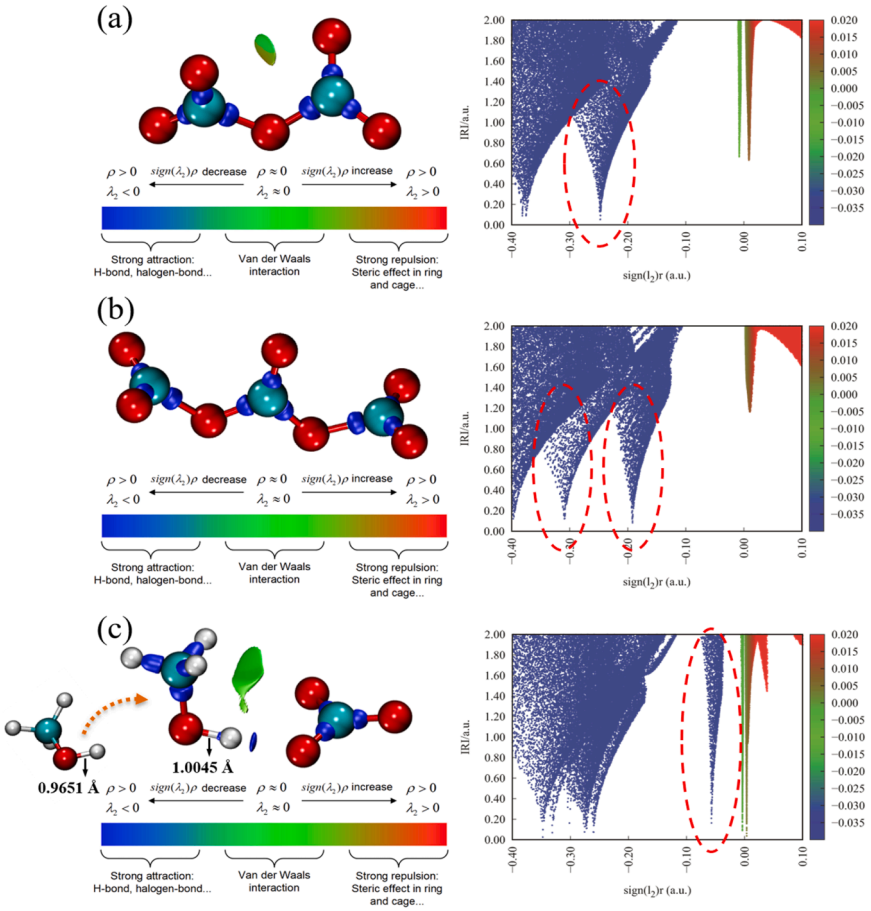

Fig. 7. IRI analysis of carbonate ion with substrate molecules: (a) CO_3^{2-}+CO_2, (b) CO_3^{2-}+2CO_2, (c) CO_3^{2-}+CH_3OH.

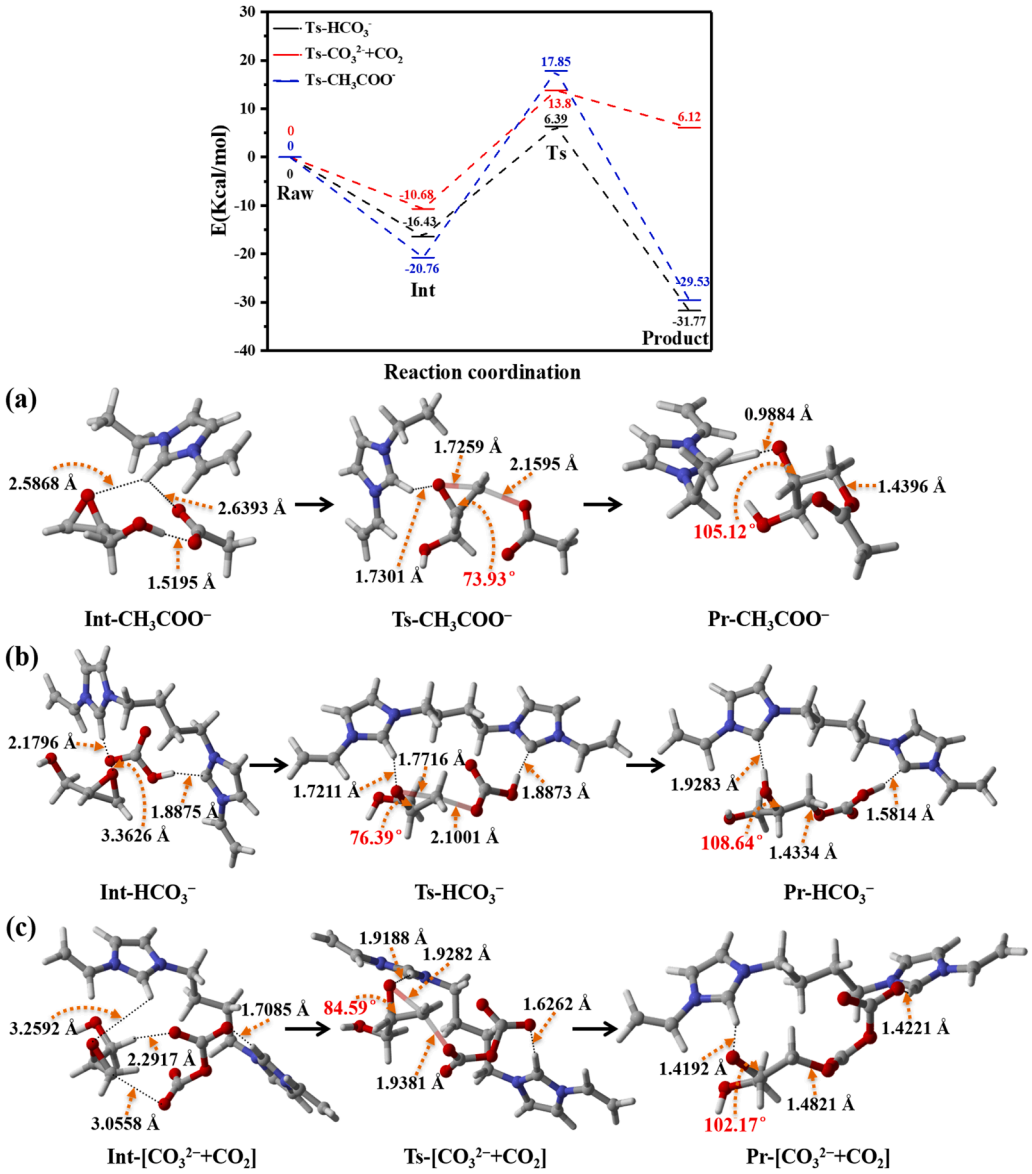

Fig. 8. Gibbs free energy distribution and transition state structure optimization of GO ring-opening process: (a) CH_3COO^- ion nucleophilic ring-opening process, (b) HCO_3^- ion nucleophilic ring-opening process, (c) $[CO_3^{2-}+CO_2]$ adduct nucleophilic ring-opening process.

position of imidazolium ring pulled the O atom of GO through hydrogen bonding (Int-CH_3COO^-), and CH_3COO^- anion attacked β-C atom of GO to form CH_3COO^--C bond (Ts-CH_3COO^-). The α-C bond angle of the ring-opening intermediate (Pr-CH_3COO^-) was enlarged to 105.12 °, and its O^- site was still stabilized by hydrogen bonding of imidazolium ring C2-H atom, awaiting electrophilic insertion of CO_2. As shown in Fig. 8b, when CO_3^{2-} anion was used for coupling reaction, due to its strong basicity, it was easy to peel off the C2-H atom of imidazolium ring to form HCO_3^- anion, which could attack β-C atom of GO to form HCO_3^--C bond (Ts-HCO_3^-), and the α-C bond angle of the ring-opening intermediate (Pr-HCO_3^-) was enlarged to 108.64° [59]. As shown in Fig. 8c, when CO_3^{2-} anion bonded CO_2 first to form $[CO_3^{2-}+CO_2]$ adduct, and then the coupling reaction proceeded, the C2-H atom of imidazolium ring could stably pull the O atom of GO (Int-$[CO_3^{2-}+CO_2]$). Subsequently, $[CO_3^{2-}+CO_2]$ adduct attacked β-C atom of GO to generate $[CO_3^{2-}+CO_2]$-C bond (TS-$[CO_3^{2-}+CO_2]$) [60]. In this process, CO_2 carried by $[CO_3^{2-}+CO_2]$ adduct could be directly inserted to form the ring-opening form of GLC (Pr-$[CO_3^{2-}+CO_2]$). Further analysis of the Gibbs free energy distribution about the ring-opening process dominated by different nucleophilic anions showed that, $\Delta G[HCO_3^-]$ = 22.82 kcal/mol < $\Delta G[CO_3^{2-}+CO_2]$ = 24.48 kcal/mol < $\Delta G[CH_3COO^-]$ = 38.64 kcal/mol, indicating that CO_3^{2-} anion in P-DPsC$_4$ImCO$_3$ had more catalytic advantages than CH_3COO^- anion in P-DPsC$_4$ImAc. Moreover, while the values of $\Delta G[HCO_3^-]$ and $\Delta G[CO_3^{2-}+CO_2]$ were similar, the energy of Pr-$[CO_3^{2-}+CO_2]$ was higher than that of Pr-HCO_3^-, attributed to the fact that the $[CO_3^{2-}+CO_2]$ adduct directly inserted the carried CO_2 into the O^- site of the ring-opening intermediate in the process of attacking GO.

Based on the above conclusions, the catalytic mechanism of P-DPsC$_4$ImCO$_3$ generating DMC through coupling reaction from diluted CO_2 was described in Fig. 9. When diluted CO_2 followed the reaction path of $[CO_3^{2-}+CO_2]$ adduct, CO_2 was co-enriched by the -SO^{3-} site and CO_3^{2-} anion. After being polarized by the hydrogen bond of C2-H atom in imidazolium ring, GO was nucleophilic attacked by $[CO_3^{2-}+CO_2]$ adduct and inserted into the carried CO_2. GLC could be formed by intramolecular cyclization of carbonate ring-opening intermediate through electrostatic action. However, when diluted CO_2 followed the reaction path of $[HCO_3^-]$ anion, the C2-H atom of imidazolium ring would be partially stripped. After GO was opened by $[HCO_3^-]$ anion, it needed to rely on the terminal O^- site of ring-opening intermediate to pull the

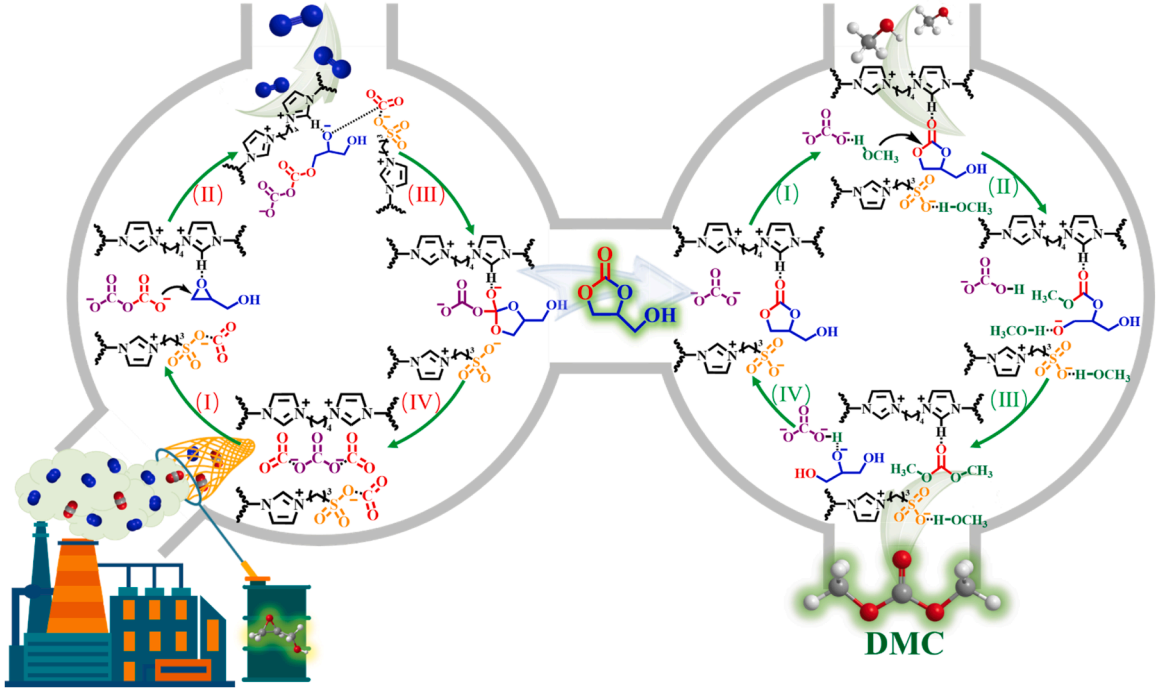

Fig. 9. Catalytic mechanism of diluted CO_2 coupling reaction.

insertion of CO_2, and cyclize to generate GLC. Subsequently, the residual flue gas after CO_2 resource utilization was released and CH_3OH was added to couple the transesterification reaction. The transesterification process also relied on the $-SO^{3-}$ site and CO_3^{2-} anion to dissociate CH_3OH for obtaining CH_3O^- anion, which attacked on GLC to synthesize DMC.

4. Conclusions

In summary, sulfonyl carbonate functionalized SC-PILs were successfully constructed by combining acidic ILs radical copolymerization with basic anions etching of PILs skeleton, which effectively promoted the synthesis of DMC through coupling reaction of diluted CO_2. Relying on the synergistic effect between the specific surface area increased by basic anions etching and the basic sites exposed by carbonate anions exchange, SC-PILs could realize the directional conversion of simulated flue gas (15% CO_2 +85% N_2) without any solvent or co-catalyst, and the DMC yield was increased from 17% to 80%. DFT theoretical calculation was used to deeply understand the activation difference of binuclear CO_3^{2-} anion on CO_2 compared with mononuclear CH_3COO^- anion and the ring-opening mechanism of [CO_3^{2-}+CO_2] adduct on epoxides.

CRediT authorship contribution statement

Jing Ding: Conceptualization, Methodology, Investigation, Writing – original draft. **Peiru Wang:** Data curation, Writing – original draft. **Yuting He:** Investigation, Writing – original draft. **Linyan Cheng:** Data curation. **Xue Li:** Software. **Cheng Fang:** Writing – review & editing. **Hongping Li:** Software. **Hui Wan:** Validation, Resources. **Guofeng Guan:** Resources, Project administration.

Declaration of Competing Interest

The authors declare that they have no known competing financial interests or personal relationships that could have appeared to influence the work reported in this paper.

Data availability

Data will be made available on request.

Acknowledgments

We deeply appreciate the support of the National Natural Science Foundation of China (Nos. 21706131, 21878159, 22078159 and 22278213) and Changzhou Key Research and Development Program (Applied Basic Research) (No. CJ20220040). We also thank the High-Performance Computing Center of Nanjing Tech University to generously offer the computational resources Finally, we sincerely thank the reviewers for their insightful and valuable suggestions.

Author contributions

The manuscript was written through contributions of all authors. All authors have given approval to the final version of the manuscript.

Appendix A. Supplementary material

Supplementary data associated with this article can be found in the online version at doi:10.1016/j.apcatb.2022.122278.

References

[1] M. McNutt, Time's up, CO_2, Science 365 (2019) 6452, https://doi.org/10.1126/science.aay8827.
[2] D. Welsby, J. Price, S. Pye, P. Ekins, Unextractable fossil fuels in a 1.5 °C world, Nature 597 (2021) 230–234, https://doi.org/10.1038/s41586-021-03821-8.
[3] L.A. Cernusak, V. Haverd, O. Brendel, D.L. Thiec, J.M. Guehl, M. Cuntz, Robust response of terrestrial plants to rising CO_2, Trends Plant Sci. 24 (2019) 578–586, https://doi.org/10.1016/j.tplants.2019.04.003.
[4] T.P. Senftle, E.A. Carter, The holy grail: chemistry enabling an economically viable CO_2 capture, utilization, and storage strategy, Acc. Chem. Res. 50 (2017) 472–475, https://doi.org/10.1021/acs.accounts.6b00479.
[5] E.C. Ra, K.Y. Kim, E.H. Kim, H. Lee, K. An, J.S. Lee, Recycling carbon dioxide through catalytic hydrogenation: recent key developments and perspectives, ACS Catal. 10 (2020) 11318–11345, https://doi.org/10.1021/acscatal.0c02930.
[6] S.H. Pyo, J.H. Park, T.S. Chang, R. Hatti-Kaul, Dimethyl carbonate as a green chemical, Curr. Opin. Green Sustain. Chem. 5 (2017) 61–66, https://doi.org/10.1016/j.cogsc.2017.03.012.

[7] P. Tundo, M. Musolino, F. Aricò, The reactions of dimethyl carbonate and its derivatives, Green Chem. 20 (2018) 28–85, https://doi.org/10.1039/C7GC01764B.

[8] A.H. Tamboli, A.A. Chaugule, H. Kim, Catalytic developments in the direct dimethyl carbonate synthesis from carbon dioxide and methanol, Chem. Eng. J. 323 (2017) 530–544, https://doi.org/10.1016/j.cej.2017.04.112.

[9] H.Z. Tan, Z.Q. Wang, Z.N. Xu, J. Sun, Y.P. Xu, Q.S. Chen, Y.M. Chen, G.C. Guo, Review on the synthesis of dimethyl carbonate, Catal. Today 316 (2018) 2–12, https://doi.org/10.1016/j.cattod.2018.02.021.

[10] S.Y. Huang, B. Yan, S.P. Wang, X.B. Ma, Recent advances in dialkyl carbonates synthesis and applications, Chem. Soc. Rev. 44 (2015) 3079–3116, https://doi.org/10.1039/C4CS00374H.

[11] D. Shi, S. Heyte, M. Capron, S. Paul, Catalytic processes for the direct synthesis of dimethyl carbonate from CO_2 and methanol: a review, Green Chem. 24 (2022) 1067–1089, https://doi.org/10.1039/d1gc04093f.

[12] Y.T. He, D. Jiang, X. Li, J. Ding, H.P. Li, H. Wan, G.F. Guan, Efficient fixation of CO_2 into carbonates by tertiary N-functionalized poly(ionic liquids): experimental-theoretical investigation, J. CO_2 Util. 44 (2021), 101427, https://doi.org/10.1016/j.jcou.2020.101427.

[13] Y.T. He, H.M. Lu, X. Li, J. Wu, T.C. Pu, W. Du, H.P. Li, J. Ding, H. Wan, G.F. Guan, Insight into the reversible behavior of Lewis-Brønsted basic poly(ionic liquid)s in one-pot two-step chemical fixation of CO_2 to linear carbonates, Green Chem. 23 (2021) 8571–8580, https://doi.org/10.1039/d1gc02539b.

[14] J.W. Maina, J.M. Pringle, J.M. Razal, S. Nunes, L. Vega, F. Gallucci, L.F. Dumée, Strategies for integrated capture and conversion of CO_2 from dilute flue gases and the atmosphere, ChemSusChem 14 (2021) 1805–1820, https://doi.org/10.1002/cssc.202100010.

[15] Y.J. Huang, G.K. Cui, Y.L. Zhao, H.Y. Wang, Z.Y. Li, S. Dai, J.J. Wang, Preorganization and cooperation for highly efficient and reversible capture of low-concentration CO_2 by ionic liquids, Angew. Chem. Int. Ed. 56 (2017) 13293–13297, https://doi.org/10.1002/ange.201706280.

[16] Z.F. Dai, Y.F. Bao, J.D. Yuan, J.Z.M. Yao, Y.B. Xiong, Different functional groups modified porous organic polymers used for low concentration CO_2 fixation, Chem. Commun. 57 (2021) 9732–9735, https://doi.org/10.1039/d1cc03178c.

[17] Y. Yamazaki, M. Miyaji, O. Ishitani, Utilization of low-concentration CO_2 with molecular catalysts assisted by CO_2-capturing ability of catalysts, additives, or reaction media, J. Am. Chem. Soc. 144 (2022) 6640–6660, https://doi.org/10.1021/jacs.2c02245.

[18] B. Jiang, Y.M. Wang, L.H. Zhang, Y.L. Sun, H.W. Yang, B.Y. Wang, N. Yang, Biodiesel production via transesterification of soybean oil catalyzed by superhydrophobic porous poly(ionic liquid) solid base, Energy Fuels 31 (2017) 5203–5214, https://doi.org/10.1021/acs.energyfuels.7b00443.

[19] W.L. Zhang, F.P. Ma, L. Ma, Y. Zhou, J. Wang, Imidazolium-functionalized ionic hypercrosslinked porous polymers for efficient synthesis of cyclic carbonates from simulated flue gas, ChemSusChem 13 (2020) 341–350, https://doi.org/10.1002/cssc.201902952.

[20] W.J. Qian, J. Texter, F. Yan, Frontiers in poly(ionic liquid)s: syntheses and applications, Chem. Soc. Rev. 46 (2017) 1124–1159, https://doi.org/10.1039/c6cs00620e.

[21] R.V. Barrulas, M. Zanatta, T. Casimiro, M.C. Corvo, Advanced porous materials from poly(ionic liquid)s: challenges, applications and opportunities, Chem. Eng. J. 411 (2021), 128528, https://doi.org/10.1016/j.cej.2021.128528.

[22] Q.W. Song, Z.H. Zhou, L.N. He, Efficient, selective and sustainable catalysis of carbon dioxide, Green Chem. 19 (2017) 3707–3728, https://doi.org/10.1039/c7gc00199a.

[23] Y. Qu, Y.L. Chen, J.M. Sun, Conversion of CO_2 with epoxides to cyclic carbonates catalyzed by amino acid ionic liquids at room temperature, J. CO_2 Util. 56 (2022), 101840, https://doi.org/10.1016/j.jcou.2021.101840.

[24] L. Guglielmero, A. Mezzetta, C.S. Pomelli, C. Chiappe, L. Guazzelli, Evaluation of the effect of the dicationic ionic liquid structure on the cycloaddition of CO_2 to epoxides, J. CO_2 Util. 34 (2019) 437–445, https://doi.org/10.1016/j.jcou.2019.07.034.

[25] F.S. Liu, Y.Q. Gu, P.H. Zhao, J. Gao, M.S. Liu, Cooperative conversion of CO_2 to cyclic carbonates in dual-ionic ammonium salts catalytic medium at ambient temperature, ACS Sustain. Chem. Eng. 7 (2019) 5940–5945, https://doi.org/10.1021/acssuschemeng.8b05997.

[26] D.F. Li, J. Li, D. Mao, H.M. Wen, Y. Zhou, J. Wang, Direct synthesis of sulfonic group tethered mesoporous poly(ionic liquid) for catalyzing deoximation reactions, Mater. Chem. Phys. 189 (2017) 118–126, https://doi.org/10.1016/j.matchemphys.2016.12.067.

[27] Z.W. Wu, C. Chen, L. Wang, H. Wan, G.F. Guan, Magnetic material grafted poly (phosphotungstate-based acidic ionic liquid) as efficient and recyclable catalyst for esterification of oleic acid, Ind. Eng. Chem. Res. 55 (2016) 1833–1842, https://doi.org/10.1021/acs.iecr.5b02906.

[28] V. Campisciano, L. Valentino, A. Morena, A. Santiago-Portillo, N. Saladino, M. Gruttadauria, C. Aprile, F. Giacalone, Carbon nanotube supported aluminum porphyrin-imidazolium bromide crosslinked copolymer: a synergistic bifunctional catalyst for CO_2 conversion, J. CO_2 Util. 57 (2022), 101884, https://doi.org/10.1016/j.jcou.2022.101884.

[29] Q.R. Guo, C. Chen, Z. Li, X. Li, H.J. Wang, N.J. Feng, H. Wan, G.F. Guan, Controllable construction of N-enriched hierarchically porous carbon nanosheets with enhanced performance for CO_2 capture, Chem. Eng. J. 371 (2019) 414–423, https://doi.org/10.1016/j.cej.2019.04.062.

[30] A. Pourjavadi, S.H. Hosseini, R. Soleyman, Crosslinked poly(ionic liquid) as high loaded dual acidic organocatalyst, J. Mol. Catal. A Chem. 365 (2012) 55–59, https://doi.org/10.1016/j.molcata.2012.08.008.

[31] A. Pourjavadi, S.H. Hosseini, M. Doulabi, S.M. Fakoorpoor, F. Seidi, Multi-layer functionalized poly(ionic liquid) coated magnetic nanoparticles: highly recoverable and magnetically separable Brønsted acid catalyst, ACS Catal. 2 (2012) 1259–1266, https://doi.org/10.1021/cs300140j.

[32] W. Yang, H.S. Li, Q. Wu, Y.J. Ren, D.X. Shi, Y. Zhao, Q.Z. Jiao, Functionalized core-shell polystyrene sphere-supported alkaline imidazolium ionic liquid: an efficient and recyclable catalyst for Knoevenagel Condensation, ACS Sustain. Chem. Eng. 8 (2020) 18126–18137, https://doi.org/10.1021/acssuschemeng.0c06467.

[33] Y.H. Bian, Q.W. Shan, C.C. Guo, C.Z. Liu, J. Zhang, Biodiesel production over esterification catalyzed by a novel poly(acidic ionic liquid)s, Catal. Lett. 151 (2021) 3523–3531, https://doi.org/10.1007/s10562-021-03592-x.

[34] Q. Wang, X.C. Cai, Y.Q. Liu, J.Y. Xie, Y. Zhou, J. Wang, Pd nanoparticles encapsulated into mesoporous ionic copolymer: efficient and recyclable catalyst for the oxidation of benzyl alcohol with O_2 balloon in water, Appl. Catal. B Environ. 189 (2016) 242–251, https://doi.org/10.1016/j.apcatb.2016.02.067.

[35] Z.J. Guo, X.C. Cai, J.Y. Xie, X.C. Wang, Y. Zhou, J. Wang, Hydroxyl-exchanged nanoporous ionic copolymer toward low-temperature cycloaddition of atmospheric carbon dioxide into carbonates, ACS Appl. Mater. Interfaces 8 (2016) 12812–12821, https://doi.org/10.1021/acsami.6b02461.

[36] Y.T. He, X. Li, W.Y. Cai, H.M. Lu, J. Ding, H.P. Li, H. Wan, G.F. Guan, One-pot multiple-step integration strategy for efficient fixation of CO_2 into chain carbonates by azolide anions poly(ionic liquid)s, ACS Sustain. Chem. Eng. 9 (2021) 7074–7085, https://doi.org/10.1021/acssuschemeng.1c01187.

[37] X.C. Wang, L.Y. Zhang, Z.J. Guo, Y.M. Shi, Y. Zhou, J. Wang, Synergistic catalysis of one-pot cascade reactions by acidic and basic binary porous polymers, Appl. Surf. Sci. 478 (2019) 221–229, https://doi.org/10.1016/j.apsusc.2019.01.217.

[38] Y.T. He, X. Li, H.P. Li, J. Ding, H. Wan, G.F. Guan, Understanding the ingenious dual role-playing of CO_2 in one-pot pressure-swing synthesis of linear carbonate, ACS Sustain. Chem. Eng. 10 (2022) 2556–2568, https://doi.org/10.1021/acssuschemeng.2c00014.

[39] J. Li, D.G. Jia, Z.J. Guo, Y.Q. Liu, Y.N. Lyu, Y. Zhou, J. Wang, Imidazolinium based porous hypercrosslinked ionic polymers for efficient CO_2 capture and fixation with epoxides, Green Chem. 19 (2017) 2675–2686, https://doi.org/10.1039/c7gc00105c.

[40] B.H. Chen, T. Ding, X. Deng, X. Wang, D.W. Zhang, S.G. Ma, Y.Y. Zhang, B. Ni, G. H. Gao, Honeycomb-structured solid acid catalysts fabricated via the swelling-induced self-assembly of acidic poly(ionic liquid)s for highly efficient hydrolysis reactions, Chin. J. Catal. 42 (2021) 297–309, https://doi.org/10.1016/S1872–2067(20)63658–0.

[41] Y.Q. Liu, K. Wang, W. Hou, W.J. Shan, J. Li, Y. Zhou, J. Wang, Mesoporous poly (ionic liquid) supported palladium(II) catalyst for oxidative coupling of benzene under atmospheric oxygen, Appl. Surf. Sci. 427 (2018) 575–583, https://doi.org/10.1016/j.apsusc.2017.08.019.

[42] L. Qin, B.S. Wang, Y.Y. Zhang, L. Chen, G.H. Gao, Anion exchange: a novel way of preparing hierarchical porous structure in poly(ionic liquid)s, Chem. Commun. 53 (2017) 3785–3788, https://doi.org/10.1039/c6cc10158e.

[43] S. Soll, P.F. Zhang, Q. Zhao, Y. Wang, J.Y. Yuan, Mesoporous zwitterionic poly (ionic liquid)s: Intrinsic complexation and efficient catalytic fixation of CO_2, Polym. Chem. 4 (2013) 5048–5051, https://doi.org/10.1039/c3py00823a.

[44] G.Y. Zhang, G.F. Wei, Z.P. Liu, S.R. Oliver, H.H. Fei, A robust sulfonate-based metal-organic framework with permanent porosity for efficient CO_2 capture and conversion, Chem. Mater. 28 (6276−6281) (2016), https://doi.org/10.1021/acs.chemmater.6b02511.

[45] W. Lu, D. Yuan, J. Sculley, D. Zhao, R. Krishna, H.C. Zhou, Sulfonate-grafted porous polymer networks for preferential CO_2 adsorption at low pressure, J. Am. Chem. Soc. 133 (2011) 18126–18129, https://doi.org/10.1021/ja2087773.

[46] Y.J. Chen, R.C. Luo, Q.L. Xu, J. Jiang, X.T. Zhou, H.B. Ji, Metalloporphyrin polymers with intercalated ionic liquids for synergistic CO_2 fixation via cyclic carbonate production, ACS Sustain. Chem. Eng. 6 (2018) 1074–1082, https://doi.org/10.1021/acssuschemeng.7b03371.

[47] W.L. Zhang, F.P. Ma, L. Ma, Y. Zhou, J. Wang, Imidazolium-functionalized ionic hypercrosslinked porous polymers for efficient synthesis of cyclic carbonates from simulated flue gas, ChemSusChem 19 (2020) 341–350, https://doi.org/10.1002/cssc.201902952.

[48] W. Hui, X.M. He, X.Y. Xu, Y.M. Chen, Y. Zhou, Z.M. Li, L.Q. Zhang, D.J. Tao, Highly efficient cycloaddition of diluted and waste CO_2 into cyclic carbonates catalyzed by porous ionic copolymers, J. CO_2 Util. 36 (2020) 169–176, https://doi.org/10.1016/j.jcou.2019.11.003.

[49] L. Liu, S. Jayakumar, J. Chen, L. Tao, H. Li, Q.H. Yang, C. Li, Synthesis of bifunctional porphyrin polymers for catalytic conversion of dilute CO_2 to cyclic carbonates, ACS Appl. Mater. Interfaces 13 (2021) 29522–29531, https://doi.org/10.1021/acsami.1c04624.

[50] J. Li, Z.J. Jia, Z.J. Guo, Y.Q. Liu, Y.N. Lyu, Y. Zhou, J. Wang, Imidazolinium based porous hypercrosslinked ionic polymers for efficient CO_2 capture and fixation with epoxides, Green Chem. 19 (2017) 2675–2686, https://doi.org/10.1039/c7gc00105c.

[51] W. Hui, X. Wang, X.N. Li, H.J. Wang, X.M. He, X.Y. Xu, Protic ionic liquids tailored by different cationic structures for efficient chemical fixation of diluted and waste CO_2 into cyclic carbonates, New J. Chem. 45 (2021) 10741–10748, https://doi.org/10.1039/D1NJ00990G.

[52] G.Y. Zhang, G.F. Wei, Z.P. Liu, S.R.J. Oliver, H.H. Fei, A robust sulfonate-based metal-organic framework with permanent porosity for efficient CO_2 capture and conversion, Chem. Mater. 28 (2016) 6276–6281, https://doi.org/10.1021/acs.chemmater.6b02511.

[53] G.Y. Zhang, H.M. Yang, H.H. Fei, Unusual missing linkers in an organosulfonate-based primitive-cubic (pcu)-type metal-organic framework for CO_2 capture and

conversion under ambient conditions, ACS Catal. 8 (2018) 2519–2525, https://doi.org/10.1021/acscatal.7b04189.
[54] T. Lu, Q.X. Chen, Interaction region indicator: a simple real space function clearly revealing both chemical bonds and weak interactions, Chem. Methods 1 (2021) 231–239, https://doi.org/10.1002/cmtd.202100007.
[55] R. Pino-Rios, D. Inostroza, G. Cárdenas-Jirón, W. Tiznado, Orbital-weighted dual descriptor for the study of local reactivity of systems with (quasi-) degenerate states, J. Phys. Chem. A 123 (2019) 10556–10562, https://doi.org/10.1021/acs.jpca.9b07516.
[56] W.H. Wang, X.X. Zhang, P. Li, Q. Sun, Z. Li, C. Ren, C. Guo, CO_2 capture and separation from N_2/CH_4 mixtures by $Co@B_8/Co@B_8^-$ and $M@B_9/M@B_9^-$ (M = Ir, Rh, Ru) clusters: a theoretical study, J. Phys. Chem. A 119 (2015) 796–805, https://doi.org/10.1021/jp511669w.
[57] S. Manzetti, T. Lu, The geometry and electronic structure of aristolochic acid: possible implications for a frozen resonance, J. Phys. Org. Chem. 26 (2013) 473–483, https://doi.org/10.1002/poc.3111.
[58] T. Lu, F.W. Chen, Multiwfn: a multifunctional wavefunction analyzer, J. Comput. Chem. 33 (2012) 580–592, https://doi.org/10.1002/jcc.22885.
[59] T. Ema, K. Fukuhara, T. Sakai, M. Ohbo, F.Q. Bai, J.Y. Hasegawa, Quaternary ammonium hydroxide as a metal-free and halogen-free catalyst for the synthesis of cyclic carbonates from epoxides and carbon dioxide, Catal. Sci. Technol. 5 (2015) 2314–2321, https://doi.org/10.1039/C5CY00020C.
[60] C. Moya, V. Sabater, G. Yagüe, M. Larriba, J. Palomar, CO_2 conversion to cyclic carbonates catalyzed by ionic liquids with aprotic heterocyclic anions: DFT calculations and operando FTIR analysis, J. CO_2 Util. 28 (2018) 66–72, https://doi.org/10.1016/j.jcou.2018.09.012.